SAND2010-0187C

Direct numerical simulation of flame stabilization downstream of a transverse fuel jet in cross-flow

R. W. Grout[1], A. Gruber[b], C. S. Yoo[c], J. H. Chen[a]

[a] *Combustion Research Facility, Livermore, California.*
[b] *SINTEF Energy Research, Trondheim, Norway.*
[c] *Ulsan National Institute of Science and Technology, Ulsan, South Korea.*

Abstract

A reactive transverse fuel jet in cross-flow (JICF) configuration is studied using three-dimensional direct numerical simulation (DNS) with detailed chemical kinetics in order to investigate the mechanism of flame stabilization in the near field of a fuel jet nozzle. JICF configurations are used in practical applications where high mixing rates are desirable between the jet and the cross-flow fluids. Classical applications of JICF configurations are fuel injection nozzles and dilution holes in gas turbine combustors. This study examines the case of a nitrogen-diluted hydrogen transverse jet exiting a square nozzle perpendicularly into a cross- flow of heated air. Improved understanding of the flame stabilization mechanism acting downstream of the transverse fuel jet will enable the formulation of more reliable guidelines for design of fuel injection nozzles characterized by minimal flame holding behavior and intrinsic flashback safety. Results show that the flame is stabilized on the downstream side of the fuel jet at the location of the vortex shedding generated by the jet shear layer. The core of the heat release is located near the trailing edge of the fuel jet, at approximately 4 nozzle diameters away from the wall, and is characterized by the simultaneous occurrence of locally stoichiometric reactants and low flow velocities in the mean. Instantaneously, upstream flame movement is observed through propagation into the outer layers of jet vortices.

Keywords:
Direct numerical simulation, transverse jet, fuel injection, flame stabilization, hydrogen combustion

1. Introduction

Global reduction of greenhouse-gases and pollutant emissions has become an important issue for the energy sector and in this respect hydrogen-rich gases have emerged as candidate fuels in pre-combustion CO_2 separation scenarios, for large scale power generation with carbon capture and storage (CCS), and in the context of coal gasification (IGCC). While gas turbine combustors burning hydrocarbon fuels in lean premixed (LPM) mode have reached a high level of maturity [1], only moderate success has been achieved by gas turbine manufacturers in developing efficient, environmental friendly, combustion chambers that burn hydrogen-rich fuels and operate safely and reliably in LPM mode [2]. One of the first and most serious design challenges for the premixer section of such hydrogen-fired combustors is the issue of fuel injection. High reactivity of the hydrogen fuel when injected into the relatively hot oxidant stream exiting the compression stage complicates identifying a fuel injection configuration that does not allow flame stabilization in the near field of the fuel injection nozzle. This is critically important, as it ensures intrinsic (passive) flashback safety of the fuel injection system: in the eventuality that an off-design transient event allows the flame to propagate upstream of its design position inside the premixer, an intrinsically safe fuel injection system is able to flush the flame out of the premixer as soon as the off-design transient has receded. A design providing anchoring locations is therefore unacceptable, so a clear understanding of the mechanism for flame anchoring in this configuration is a valuable design aid.

The objective of the present work is to identify the mechanism of flame anchoring in the wake of a transverse fuel jet in cross-flow (JICF) by examining the interplay of flame structure and propagation characteristics with the flow and mixing fields in the near field of the fuel nozzle. Identifying the physical mechanism behind flame anchoring is vitally important to develop more reliable design guidelines for safe fuel injection. JICF configurations are characterized by a high degree of unsteadiness and by large-scale coherent vortical structures that form in the wake of the transverse jet [3]. These structures stretch the interface and increase the area available for molecular mixing which increases the mixing rate, facilitating combustion. Previous DNS studies of inert JICF configurations [4, 5, 6, 7, 8] have shown that several factors, e.g.: the momentum ratio between the transverse jet and the cross flow, the shape of the nozzle, the angle of injection, the thickness of the approaching cross-flow boundary layer, influence the flow and scalar mixing fields. Further, Hasselbrink and Mungal [9] showed observed experimentally that

heat release in a reacting case can influence the overall rate of cross flow fluid entrainment.

Direct numerical simulation (DNS) of the reactive JICF studied here provides detailed information about the flow structures and turbulence-chemistry interaction which facilitate flame stabilization. In addition to fully resolving the turbulent velocity fields, the two-way coupling between the heat release and the flow field is accurately accounted for using multi-step chemical kinetics [10] and molecular transport mechanism. DNS is uniquely capable of providing the necessary information about the turbulent flow and on its interaction, at a microscale level, with combustion chemical kinetics. The numerical simulation presented here, characterized by a square jet nozzle geometry, is the first part of a parametric study of inert and reactive JICF configurations that includes several other nozzle shapes, injection angles, momentum ratios and turbulence levels.

The remainder of this paper is organized as follows: Section 2 gives an overview of the numerical method and case configuration. Section 3 presents the key results in the context of the stabilization mechanism. Finally, Section 4 summarizes the main findings and provides an outline of future planned work.

2. Mathematical Description And Configuration

The Navier-Stokes equations in their compressible formulation are solved on a 3-D computational domain using the finite-difference solver S3D [11]. The boundary conditions are configured to simulate a turbulent flame stabilized in the wake of a transverse laminar fuel jet exiting a blunt squared nozzle[1] orthogonally into a turbulent boundary layer cross flow over a flat plate. The wall is assumed inert and no surface reactions are considered while gas-phase low-temperature recombination reactions of radical species at the wall are taken into account. The mechanism from [10] is used to represent hydrogen-air chemical kinetics including 9 species and 19 reactions.

Figure 1 depicts an instantaneous illustration of the solution and includes volume renderings of the hydrogen, temperature and HO_2 radical scalar fields.

The turbulent cross flow enters the computational domain from a non-reflecting inflow boundary. As the cross flow direction is not homogeneous in the presence of the transverse jet and of

[1]The choice of the squared nozzle shape for the first part of the ongoing parametric study is motivated by its simplicity in the context of the Cartesian grids used in DNS.

the flame, the recycling procedure described in [12] cannot be used. Therefore, an auxiliary DNS of an inert turbulent flow over a flat plate is used to provide the reactive case with the initial turbulent field and inlet turbulence. The auxiliary simulation is performed at lower resolution ($\Delta \sim 100\mu m$); the auxiliary grid is comprised of $384 \times 240 \times 300$ points spanning physical dimensions 40mm × 20mm × 20mm in the x,y,z directions. Periodic boundary conditions are applied in the spanwise and streamwise directions and the flow is driven by a body force acting in the streamwise direction. The viscous length scale is measured *a posteriori* as $\delta_\nu = 35.4\,\mu m$ and the friction velocity $u_\tau = 2.1 m/s$. Since the domain length is $> 1000\delta_\nu$, we expect it to be sufficiently large to adequately capture the boundary layer structures necessary for realistic feed data. After 4 flow through times based on the mean cross flow velocity ($u_{\mathrm{cf}} = 55 m/s$) a realistic boundary layer is established and sampled over continued evolution. Although the turbulent feed data is time evolving, the increase in the boundary layer thickness is very small between the start and end times of the main flame simulation. The boundary conditions are implemented following the method described in [13] and [14], including the successful improvements of [15] and [16]. For the main simulation, the boundary conditions are: non-reflecting at the inflow ($x = 0$) and outflow ($x = L_x$,$y = L_y$) planes, no-slip isothermal solid surface at the wall boundary ($y = 0$), and periodic in the spanwise direction ($z = 0$ and $z = L_z$). The temperature of the wall and of the cross flow air is set to 750 K while the fuel jet temperature is set to 420 K.

2.1. Reacting DNS

The three-dimensional Cartesian grid used for the production simulation is uniform in the stream-wise and span-wise directions and is refined in the wall-normal direction near the solid surface using a *tanh* mapping. The production grid is comprised of $1.6 \cdot 10^9$ points arranged as $1408 \times 1080 \times 1100$ in the x,y,z directions with physical domain dimensions 25mm × 20mm × 20mm. The first point off the wall is at $y^+ = 0.33$ where the superscript + indicates non-dimensionalization by the viscous length scale δ_ν computed from the feed data. The production grid resolution is $\Delta x^+ \sim 0.5$ ($\Delta x = 17.8\ \mu$m), $\Delta y^+ \sim 0.3$–0.7 ($\Delta y = 10.2$–$24.3\,\mu$m) and $\Delta z^+ \sim 0.5$ ($\Delta z = 18.2\mu$m). The simulation is run on 48 000 cores of *Jaguar*, the Cray XT5 at ORNL, and used approximately 4M cpu hours.

The velocity field for the production simulation is initialized with the velocity field present in the auxiliary domain at the instant the feed data sampling was started. After transitioning the jet inlet velocity to its final value over $10\mu s$, the simulation is advanced an additional flow-through

time to establish the fuel plume. Next, reaction is enabled and a 'flame anchor', consisting of a notional heated rod, is placed in the flow to coincide with flammable mixture for only 8 μs before it is removed. Once all of the fluid present in the domain when the flame anchor is removed exits through the outflow boundary, the solution is up-sampled to the production grid.

3. Results and Discussion

In light of the the importance of the stabilization mechanism for combustor design, we will discuss the results first in terms of the mean flame stabilization. In the latter part of this section we will explore flame behaviour from the perspective of mixture preparation and flow structures resulting from the jet/boundary layer flow interaction.

3.1. Mean flame stabilization

Time averages of the mean quantities were accumulated over a 0.4ms window using 50 snapshots of the solution saved at $8\mu s$ intervals. The resulting time averaged solution on the midplane in the spanwise direction is shown in the top (mixture fraction, normalized heat release rate) and bottom (normalized heat release rate, velocity magnitude) parts of Figure 2. From the heat release contours, we can see that the flame stabilizes, on average, at 1.5–2 jet widths downstream and 3–5 jet heights from the jet exit. The peak heat release is coincident with a region where the magnitude of the average flow velocity is locally low and the average mixture fraction $\overline{\zeta} = 0.171$ is near stoichiometric (the stoichimetric mixture fraction is $\zeta_{\mathrm{st}} = 0.169$). The isolines in Figure 3 show where the magnitude of the mean velocity falls below 25m/s, or approximately 10% of the maximum velocity in the domain; the vectors indicate the in-plane velocity. In the spanwise direction, the peak heat release is located on the center-line, just above and between the large counter-rotating vortex pair which has been identified in non-reactive jet-in-cross-flow studies [3] as contributing significantly to mixing between the jet and cross-flow fluids [8].

3.2. Mixture preparation

The mean stabilization location suggests that the stabilization mode may be via partially premixed flame propagation in a region where the advective velocity is low enough to allow the flame to, on average, obtain equilibrium.

The instantaneous solution is shown on the midplane in Figure 4 where the mixture fraction ζ, is overlayed with contours of instantaneous heat release. The mixture fraction is computed

using the hydrogen and oxygen elemental mass fractions. In Figure 5, the Takeno flame index, mixture fraction scalar dissipation rate ($\chi \equiv 2D\nabla\xi \cdot \nabla\xi$), and a topological flow classification (discussed in the following section) are shown for the same slice as Figure 4, enlarged to show the mean field more clearly. The mixture fraction scalar dissipation rate is non-negligible even in the far field, and especially where the heat release is significant. At the same time, the Takeno flame index [17], for this flame defined as:

$$\mathrm{FI} \equiv \frac{\nabla Y_{H2} \cdot \nabla Y_{O2}}{|\nabla Y_{H2}||\nabla Y_{O2}|}, \tag{1}$$

indicates that the gradients of the fuel and oxidizer are largely aligned in the reaction zone.

Although the state of the mixture preparation alone does not permit the combustion mode to be definitively identified, taken together with the presence of thin regions with significant heat release where the fuel and oxidizer gradients are aligned suggests that flame propagation is an important phenomena in this flame. Taken alone, the co-location of the peak mean heat release with the low mean velocity region discussed earlier is inconclusive; either ideal mixture preparation and mixing rates for a diffusion flame or a stabilized (stratified) premixed flame could produce similar results. However, in light of the instantaneous mixture preparation data, stratified premixed flame propagation is indicated.

The flame is strongly modulated by the velocity field; near the location where the jet breaks up, tendrils of the flame can be seen which are drawn into the vortical flow structures from the jet shear-layer instability. In the sequence of snapshots shown in Figure 5, there is conspicuous interaction between the flame and the flow structures associated with the fuel jet.

3.3. Significant flow topological structures

Identification of the local nature of the flow can be somewhat ambiguous. Chong et al. proposed classification of critical points in a local reference frame through analysis of the invariants of the rate-of-deformation tensor [18]. Through these invariants, the local flow structure can be identified as one of 27 fundamental types categorized by Chong et al. for a variable density flow; interestingly, for this flow, only a few dominant types are present as shown in Figure 5; these are listed in Table 2 along with the canonical description enumerated by Chong et al.

Some of these elementary types can be elucidated by considering a 'canonical' vortex; Figure 6 shows a significantly enlarged flow feature interacting with the flame. The identified vortex, with large vorticity magnitude at it's core, can be seen in the classification with a coherent FC/U

region surrounded by 'arms' of FS/S and NSS/U. Tanahashi et al. [19] used only the 'Q' velocity invariant to separate strain dominated regions ($Q < 0$) from coherent fine scale eddies ($Q > 0$) in a premixed flame; in this particular structure, the regions where $Q < 0$ are found outside the structure and within the 'arms', where the flow classification is the NSS/U topology which is indicative of the quintessential laminar strained flame. It is also in this region where the heat release suggests the flame is being 'wrapped up' and strained by the vortex.

From the sequence in Figure 5, we can make several qualitative observations:

1. The vortical structures prior to the jet breakup are clearly represented by a core FC/U structure surrounded by 'arms' with FS/S structure
2. The vortical structures in the jet breakup show a similar FC/U core + FS/S arrangement, but the shape is significantly distorted
3. The lengthscale of the flow structures grows noticeably across the flame
4. *The most upstream point of the flame is in the vicinity of where the breakup of the flow structures begins*
5. *The flame front is most diffuse and penetrated by small vortical structures in the breakup zone*
6. *The flame front appears thinnest in the regions where there is a contiguous region of NSS/U topology*

The final three observations are worthy of note: while the NSS/U topological configuration is the quintessential notion of a flamelet, the diffuse flame penetrated by small flow structures is consistent with the notion of the broken reaction zone [20]. This has significant implications for modeling this configuration in that for phenomenological models, the appropriate canonical configuration varies throughout the domain.

To look quantitatively at the relationship between the flame front and the flow topology, a progress variable defined with reference to the local mixture fraction is a useful flame marker which is frequently used for stratified premixed flames, e.g. [21]:.

$$c \equiv \frac{Y_{H_2O} - Y_{H_2O,u}(\xi)}{Y_{H_2O,b}(\xi) - Y_{H_2O,u}(\xi)}, \tag{2}$$

where the burnt and unburnt states are defined with respect to an appropriate reference configuration. Here, we chose complete combustion for the burnt reference state — this is not necessarily an appropriate choice for modelling purposes, but gives us a suitable marker for the

flame position. The magnitude of the the gradient of the progress variable is closely related to the thickness of the flame front. In Figure 7 we have computed the average of the magnitude of the progress variable gradient and the heat release rate conditional on three quantities: the local mixture fraction, progress variable as defined by Equation (2), and the topological classification. As expected, the flow topology typically associated with a canonical laminar flamelet (green) has relatively high gradient magnitude, suggesting a flame front thinned by flow straining as observed by Tanahashi et al. [19]. This mode also displays slightly increased heat release rates amongst the flow topologies which contribute most significantly to the overall heat release (NSS/U, FS/S, NSS/S, FC/U). Interestingly, the portions of the flame with NNN/U topology have relatively low progress variable gradients indicating a thickened flame front but high heat release, suggesting that these types of flow structures penetrate the flame front and make it more diffuse.

4. Concluding Remarks

Analysis of a DNS solution for a reacting JICF configuration indicates that the flame stabilizes in a low velocity region between the large counter-rotating vortex pair where the mixture is near stoichiometric. Strong jet vortices are observed to have 'arms' of focus / stretching (stable) separated from the core by node/saddle/saddle (unstable) regions. The upstream portion of the flame propagates into the vortices preferentially through these regions. In the far field, the highest heat release rates are found in regions with node/node/node (unstable) configuration where the progress variable gradient is lower, suggesting penetration of the flame by small vortices is important. Taken together, these observations have important implications for accurate modelling of this configuration in the RANS sense, suggesting that models accounting for stratified premixed combustion in the broken reaction zones regime may be necessary. Future simulations are planned to investigate other nozzle shapes and inclined injection; these arrangements, expected to produce less intense jet vortices, will be used to verify that the flame is less prone to anchor as these features become less pronounced.

Acknowledgements

Computational support for this project was supported by and this research used resources of the National Center for Computational Sciences at Oak Ridge National Laboratory, which

is supported by the office of Science of the US Department of Energy under contract DE-AC05-00OR22725. The work at Sandia National Laboratories was supported by the Division of Chemical Sciences, Geosciences, and Biosciences, Office of Basic Energy Sciences of the US Department of Energy and by the US Department of Energy SciDAC Program. SNL is a multiprogramme laboratory operated by Sandia Corporation, a Lockheed Martin Company for the US DOE under Contract DE-AC04-94AL85000. The authors would like to acknowledge the help of Dr. Hongfeng Yu in preparing the volume rendering in Figure 1. The work at SINTEF is supported by the Climit Program of the Research Council of Norway and Gassnova.

References

[1] K. Döbbeling, J. Hellat and H. Koch, "25 Years of BBC/ABB/Alstom Lean Premix Combustion Technologies", *ASME Journal of Engineering for Gas Turbines and Power*, 129 (2007) 2–12.

[2] P. Chiesa, G. Lozza, and L. Mazzocchi, "Using Hydrogen as Gas Turbine Fuel", *ASME Journal of Engineering for Gas Turbines and Power*, 127 (2005) 73–80.

[3] T.F. Fric and A. Roshko, "Vortical Structure in the Wake of a Transverse Jet", *Journal of Fluid Mechanics*, 279 (1994) 1–47.

[4] S. Muppidi and K. Mahesh, "Study of Trajectories of Jets in Crossflow Using Direct Numerical Simulations", *Journal of Fluid Mechanics*, 530 (2005) 81–100.

[5] S. Muppidi and K. Mahesh, "Two-Dimensional Model Problem to Explain Counter-Rotating Vortex Pair Formation in a Transverse Jet", *Physics of Fluids*, 18 (2006) 085103-1–9.

[6] S. Muppidi and K. Mahesh, "Direct Numerical Simulation of Round Turbulent Jets in Crossflow", *Journal of Fluid Mechanics*, 574 (2007) 59–84.

[7] S. Muppidi and K. Mahesh, "Direct Numerical Simulation of Passive Scalar Transport in Transverse Jets", *Journal of Fluid Mechanics* 598 (2008) 335–360.

[8] M. Salewski, D. Stankovic and L. Fuchs, "Mixing in Circular and Non-circular Jets in Crossflow", *Flow, Turbulence and Combustion*, 80 (2008) 255–283.

[9] E.H. Hasselbrink and M.G. Mungal, "Transverse jets and jet flames. Part 2. Velocity and OH field imaging", *Journal of Fluid Mechanics*, 443 (2001) 27–68.

[10] J. Li, Z. Zhao, A. Kazarov and F.L. Dryer, "An Updated Comprehensive Kinetic Model of Hydrogen Combustion", *International Journal of Chemical Kinetics*, 36 (2004) 566–575.

[11] J.H. Chen, A. Choudhary, B. de Supinski, M. DeVries, E.R. Hawkes, S. Klasky, W.K. Liao, K.L. Ma, J. Mellor-Crummey, N. Podhorski, R. Sankaran, S. Shende and C.S. Yoo, "Terascale direct numerical simulations of turbulent combustion using S3D", *Computational Science and Discovery*, 1 (2008).

[12] P.R. Spalart, M. Strelets and A. Travin, "Direct Numerical Simulation of Large-Eddy-Break-Up Devices in a Boundary Layer", *International Journal of Heat and Fluid Flow*, 27 (2006) 902–910.

[13] K. W. Thompson, *Journal of Computational Physics*, 68 (1987) 1–24.

[14] K. W. Thompson, *Journal of Computational Physics*, 89 (2) (1990) 439–461.

[15] T. Poinsot and S. K. Lele, *Journal Computational Physics*, 101 (1) (1992) 104–139.

[16] J. C. Sutherland, and C. A. Kennedy, *Journal of Computational Physics*, 191 (2003) 502–524.

[17] H. Yamashita, M. Shimada and T. Takeno, "A numerical study on flame stability at the transition point of jet diffusion flames", *Proceedings of the Combustion Institute* 26 (1996) 24–34.

[18] M.S. Chong, A.E. Perry, and B.J. Cantwell, "A general classification of three-dimensional flow fields", *Phys. Fluids A* 2(5) (1990) 765–777,

[19] M. Tanahashi, M. Fujimura and T. Miyauchi, "Coherent fine-scale eddies in turbulent premixed flames", *Proceedings of the Combustion Institute* 28 (2000) 529–535.

[20] N. Peters *Turbulent Combustion* Cambridge University Press (2000).

[21] K. Bray, P. Domingo and L. Vervisch, "Role of the progress variable in models for partially premixed turbulent combustion", *Combustion and Flame*, 141 (2005) 431–437.

Tables

$\mathrm{Re}_{\mathrm{jet}}$	$\mathrm{T}_{\mathrm{jet}}$	T_{cf}	u_j/u_{cf}	$\sqrt{\rho_j u_j^2/\rho_{cf} u_{\mathrm{cf}}^2}$	$u'_{\mathrm{cf}}/u_{\mathrm{cf}}$
3980	423k	750k	4.5	3.4	0.1

Table 1: Simulation parameters ($\mathrm{Re}_{\mathrm{jet}}$ is based on hydraulic diameter)

Topological Classification	Description
2 (blue)	Node / node / node, unstable (NNN/U)
11 (dark green)	Node / saddle / saddle, stable (NSS/S)
12 (bright green)	Node / saddle / saddle, unstable (NSS/U)
18 (yellow)	Focus / stretching, stable (FS/S)
19 (light orange)	Focus / stretching, unstable (FS/U)
20 (red)	Focusing / compressing, stable (FC/S)
21 (orange)	Focusing / compressing, unstable (FC/U)

Table 2: Dominant flow topological classifications

Figures

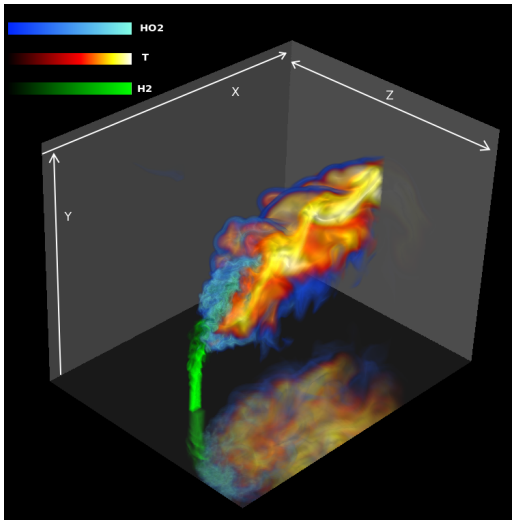

Figure 1: Volume rendering of temperature (black body colormap), HO_2 (blue colormap), and H_2 (green colormap) scalar fields at t=2.802ms from start of simulation. Opacity transfer functions adjusted to highlight the regions with high temperature, HO_2, or H_2 mass fraction.

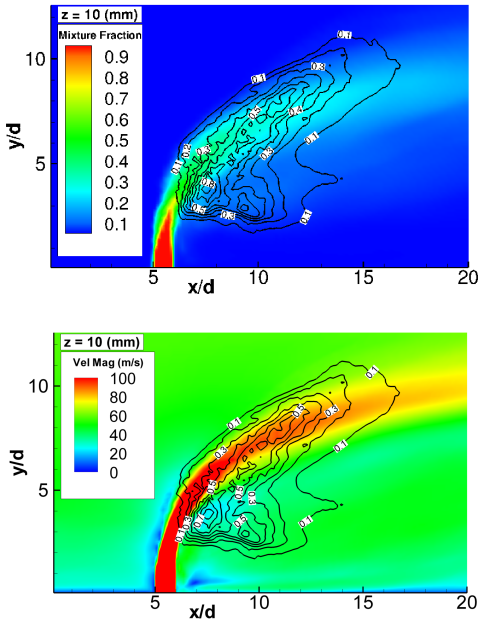

Figure 2: Slices on the midplane showing RANS averaged solution for mixture fraction and normalized heat release rate (top) and velocity magnitude and normalized heat release rate (bottom).

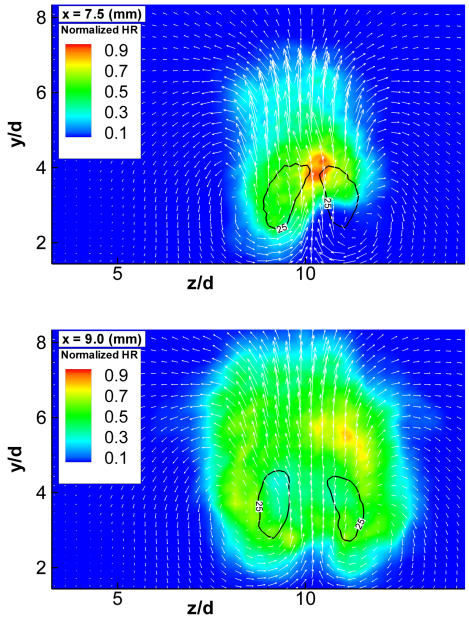

Figure 3: Slices orthogonal to mean flow direction showing RANS averaged solution for heat release rate normalized by peak heat release rate, in-plane velocity vectors, and isolines for the mean velocity magnitude.

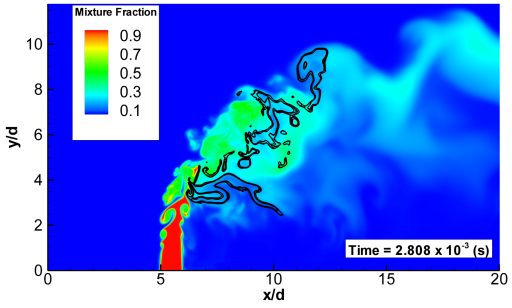

Figure 4: Slice on the midplane showing instantaneous mixture fraction at t=2.808ms. Lines represent $8 \cdot 10^9$ and $1 \cdot 10^{10} J/m^3/s$ isocontours of the instantaneous heat release rate.

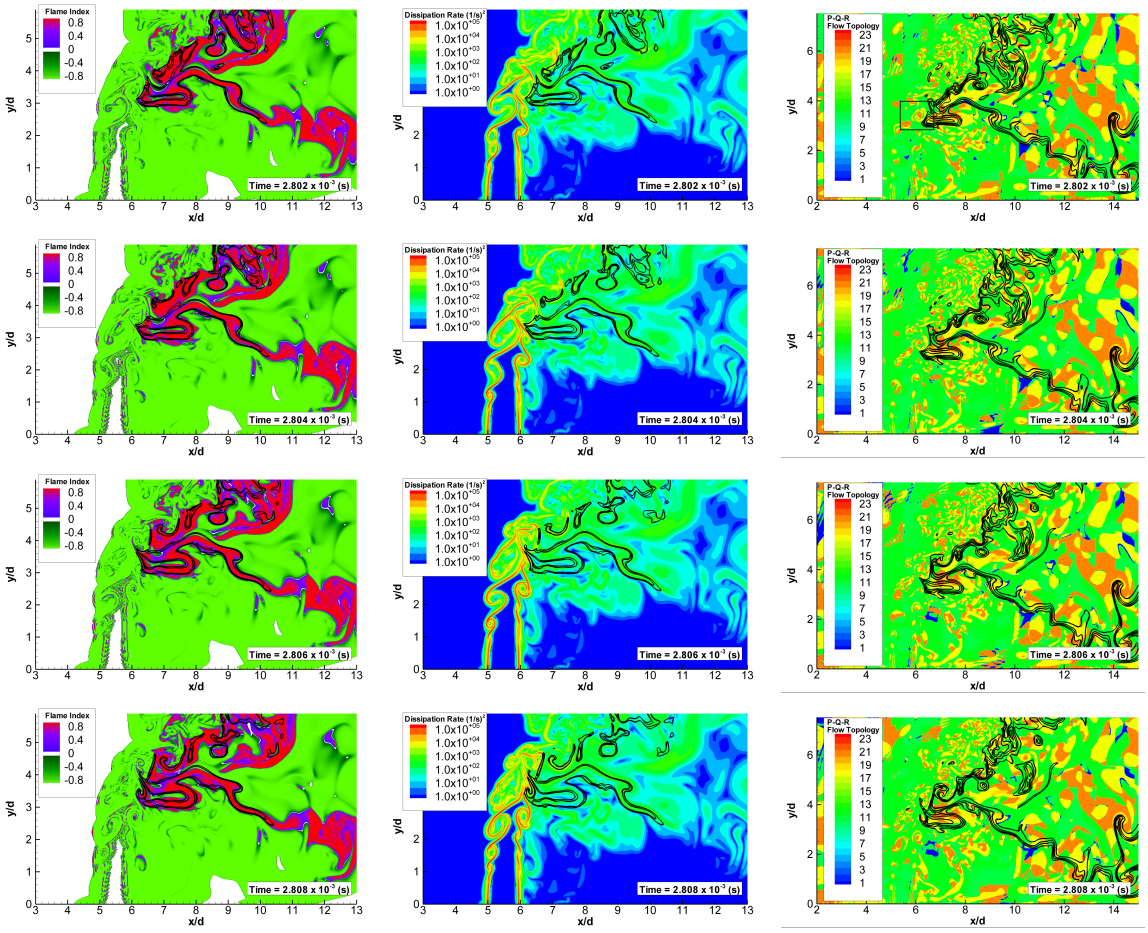

Figure 5: Instantaneous snapshots of normalized flame index, scalar dissipation rate, and flow topology classification. Lines in left and middle represent $8 \cdot 10^9$ and $1 \cdot 10^{10} J/m^3/s$ (approximately one-half of peak) isocontours of the instantaneous heat release rate. On right, lines are isocontours of progress variable range from 0.2–0.8.

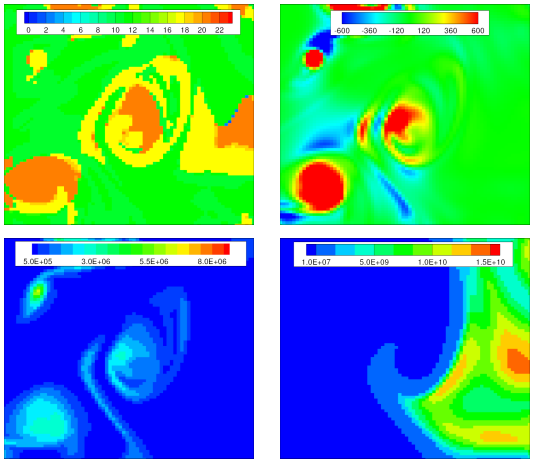

Figure 6: Canonical flow structure at $t = 2.802$ms colored by classification (top left), 'Q' invariant (top right), enstrophy (bottom left), and heat release rate (bottom right). Colorscale for Q invariant saturates at end of labelled range to clarify sign of Q. Regions shown are indicated by the inset box in Figure 5.

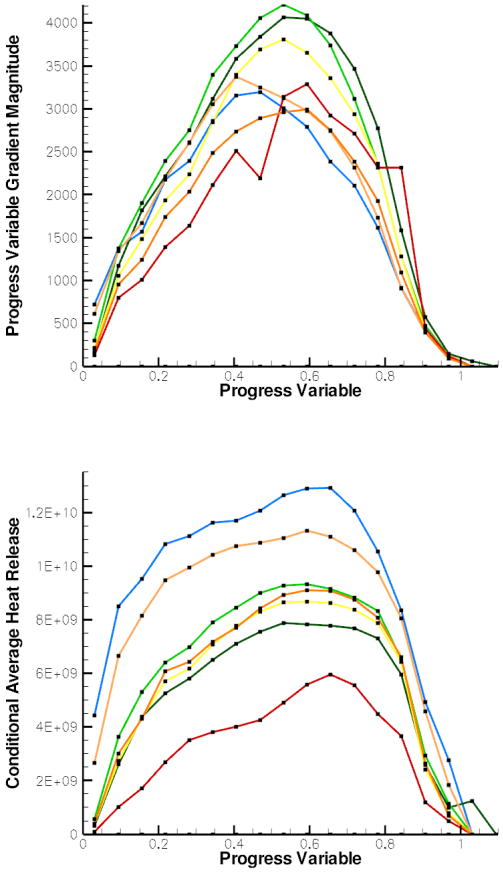

Figure 7: Conditionally averaged magnitude of progress variable and heat release rate. Averages are conditional on mixture fraction $0.2 < \xi < 0.4$, progress variable (50 equally sized intervals), and the flow classification; lines shown are colored by the flow topology as given in Table 2.

Figure captions

Figure 1: Volume rendering of temperature (black body colormap), HO_2 (blue colormap), and H_2 (green colormap) scalar fields at t=2.802ms from start of simulation. Opacity transfer functions adjusted to highlight the regions with high temperature, HO_2, or H_2 mass fraction.

Figure 2: Slices on the midplane showing RANS averaged solution for mixture fraction and normalized heat release rate (top) and velocity magnitude and normalized heat release rate (bottom).

Figure 3: Slices orthogonal to mean flow direction showing RANS averaged solution for heat release rate normalized by peak heat release rate, in-plane velocity vectors, and isolines for the mean velocity magnitude.

Figure 4: Slice on the midplane showing instantaneous mixture fraction at t=2.808ms. Lines represent $8 \cdot 10^9$ and $1 \cdot 10^{10} J/m^3/s$ isocontours of the instantaneous heat release rate.

Figure 5: Instantaneous snapshots of normalized flame index, scalar dissipation rate, and flow topology classification. Lines in left and middle represent $8 \cdot 10^9$ and $1 \cdot 10^{10} J/m^3/s$ (approximately one-half of peak) isocontours of the instantaneous heat release rate. On right, lines are isocontours of progress variable range from 0.2–0.8.

Figure 6: Canonical flow structure at t = 2.802ms colored by classification (top left), 'Q' invariant (top right), enstrophy (bottom left), and heat release rate (bottom right). Colorscale for Q invariant saturates at end of labelled range to clarify sign of Q. Regions shown are indicated by the inset box in Figure 5.

Figure 7: Conditionally averaged magnitude of progress variable and heat release rate. Averages are conditional on mixture fraction $0.2 < \xi < 0.4$, progress variable (50 equally sized intervals), and the flow classification; lines shown are colored by the flow topology as given in Table 2.